Relationship between microstructures and optoelectronic properties of Ag-O-Cs photoemitting surfaces: The *S*-1 photocathode

Quark Y. Chen and Clayton W. Bates, Jr.
Department of Materials Science and Engineering, Stanford University, Stanford, California 94305-2205
(Received 1 June 1987)

The *S*-1 photocathode is a prime example of a heterogeneous composite whose optical and electronic transport properties have been measured by many researchers. It provides an excellent system for testing theories of composites which replace a heterogeneous system of individual components having different physical properties with a homogeneous one having averaged physical properties depending on those of the components, the so-called effective-medium approximation. Using a recently formulated self-consistent dynamic effective-medium approximation that reduces to the requirement that ϵ_{eff} be chosen so that the forward scattering amplitude of the particles embedded in the medium should vanish on the average, we present a theoretical investigation of the optical, electronic-transport, and photoemission behavior of *S*-1 photocathodes with various microstructures. From an analysis of the relation $\epsilon_{\text{eff}}=(\epsilon_1)_{\text{eff}}+i(\epsilon_2)_{\text{eff}}$, the quality factor $Q=(\epsilon_1)_{\text{eff}}/(\epsilon_2)_{\text{eff}}$, and the optical-energy-loss function $-\text{Im}(1/\epsilon_{\text{eff}})$, it is found that the photoelectric-quantum-yield (PQY) peak between 3800 and 4100 Å is caused by a dielectric anomaly due to the collective oscillation of free electrons in isolated small Ag particles embedded in a host matrix of unitary dielectric constant. The broad peak in the PQY centered near 8000 Å corresponds to a surface-mode collective oscillation of free electrons in the aggregated Ag particles, which surround the host matrix, with $\epsilon=1$. The minimum around 3.8 eV in PQY is due to plasmon loss. A multiple-step model of photoemission from *S*-1 photocathodes is constructed to calculate the PQY using only the experimentally determined energy-dependent electron mean free path and energy barriers at interfaces. This model includes multiple elastic scattering of photoexcited electrons in Ag particles, which can completely account for the magnitude of enhanced photoyields from small-metal-particle systems. With this model, calculated PQY curves for various microstructures are presented to show their effects on the photoelectric threshold and magnitude of the PQY throughout the entire optical region. This calculation yields quantitative results that fit experimental data without any adjustable factors.

I. INTRODUCTION

Since the *S*-1 photocathode was discovered in 1929 (Ref. 1) a tremendous amount of work has been performed in an effort to understand its mechanism of photoemission. Most of the research on this surface up to 1968 is discussed by Sommer.[2] In a more recent publication,[3] we proposed a microstructural model of the *S*-1 consisting essentially of a base layer of Ag microparticles coated with $Cs_{11}O_3$ in a matrix of Cs_2O ($\epsilon=4.0$), with a surface layer of $Cs_{11}O_3$-coated Ag microparticles in vacuum ($\epsilon=1$). The most photoelectronically active Ag microparticles were determined to be on the order of 50 Å in diameter, produced near and on the surface by the heating employed in the photocathode processing. Figures 1(a) and 1(b) show, respectively, the electronic energy bands and microstructure for this system. This model is based upon the results of x-ray photoelectron spectroscopy[4–6] (XPS) and Raman spectroscopy[7] measurements. The microstructure was considered to consist of two units, $Cs_{11}O_3$-coated Ag microparticles surrounded by medium, and medium surrounded by $Cs_{11}O_3$-coated Ag microparticles. These two types of microstructural units were first used by Sheng to describe the optical properties of Au-SiO_2 granular composites.[8] The response to electromagnetic radiation of these types of microstructures is discussed by Bohren and Huffman.[9] To account for the photoelectric quantum yield (PQY) of the *S*-1 in the near infrared we found it necessary to include in a relative breakdown of these two basic structural units at least 2% of the microstructural unit consisting of $Cs_{11}O_3$-coated Ag microparticles surrounding the medium in addition to the unit of medium surrounding the $Cs_{11}O_3$-coated Ag microparticles. Further, our calculations indicate (Sec. II) that the surface layer in the *S*-1 is the major contributor to the PQY throughout its spectrum. In 1976, Ebbinghaus, Braun, and Simon[10] proposed a model of the *S*-1 which for the first time indicated the presence of $Cs_{11}O_3$ along with Ag. Their ultraviolet-photoemission-spectroscopy measurements did not indicate the presence of Cs_2O presumably because the electron escape depth using the He I resonance line at 21.2 eV was too shallow to detect it.[3,11] But it is not clear from their work whether they actually produced an *S*-1 surface, or what structural relationship existed between the Ag and $Cs_{11}O_3$, as we show in our model. These considerations aside it is interesting that in their model of the *S*-1 they attribute the PQY to Ag and $Cs_{11}O_3$ in vacuum ($\epsilon=1$) whereas in our model the major contribution to the PQY is due to $Cs_{11}O_3$-coated Ag microparticles in two structural

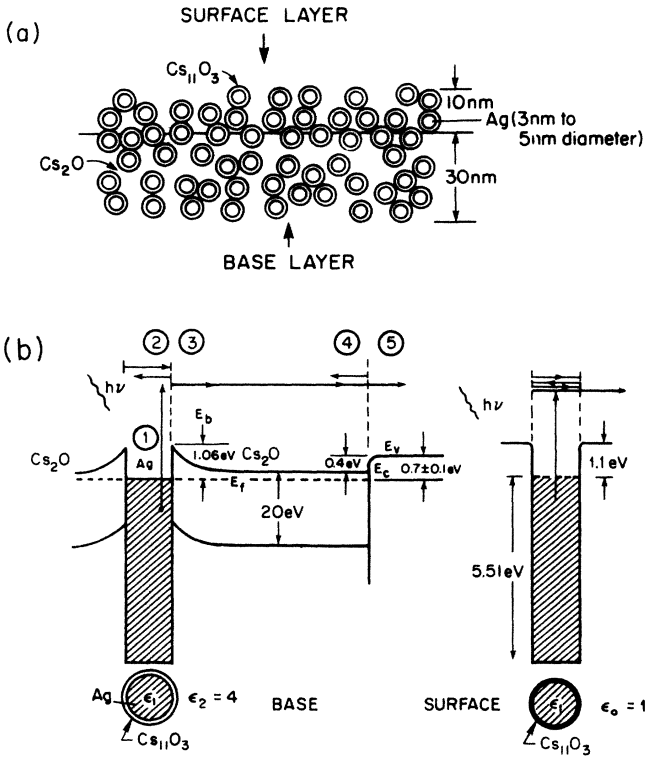

FIG. 1. (a) Microstructure and (b) energy band diagram for the *S*-1 photocathode.

configurations in a medium with $\epsilon=1$.

Wu[12,13] constructed an "equivalent-diameter particle" theory to explain the PQY of the *S*-1 in the near infrared only and found that the equivalent diameter that fit the experimental data best was about 31 Å in fair agreement with our value of 50 Å. However, Wu's electron-transport function which we also used to calculate our PQY (Ref. 3) left an undetermined adjusting factor which was necessary to bring experiment and theory into close agreement.

In Sec. II of this paper we present a multiple-step free-electron theory of photoemission which explains the PQY of *S*-1 photocathodes over their complete spectral range without any adjustable factors. Included in this theory and essential to a description without adjustable parameters is a model in which photoexcited electrons in small metal particles are scattered elastically from the boundaries and travel inelastically within.[14]

In order to understand the relationship between the microstructure and the optoelectronic behavior of the *S*-1 photocathode as a function of photon energy, we have to look further into its optical properties. This is accomplished in Sec. III by analyzing the effective dielectric constant, optical loss function and quality factor of the surface layer which, as discussed earlier is the main contributor to the PQY. By so doing, we are able to interpret the characteristics of the PQY curves of the *S*-1 photocathode as a function of photon energy and microstructure. From this theoretical study, some material-design rules can be inferred. According to these rules, one can systematically search for other heterogeneous materials for optical and optoelectronic applications.

II. MULTIPLE-STEP MODEL OF PHOTOEMISSION

The *S*-1 photocathode is composed of a surface layer ($\sim$100-Å thick) residing on a base layer ($\sim$300-Å thick), as shown in Fig. 1(a). We first look at the base layer with Ag particles embedded in a matrix of Cs_2O [Fig. 1(a)]. In this layer, the multiple-step model takes into account (1) the excitation of the electrons in the metal particles; (2) the transport of photoexcited electrons to the interfaces between the metal particles and the Cs_2O; (3) the transmission and escape (penetration) of the photoexcited electrons through the Schottky barrier (Ag-Cs_2O interface) into the Cs_2O; (4) transport of the transmitted photoexcited electrons to the Cs_2O-vacuum interface; and (5) the transmission and escape of the electrons into the vacuum which then become the photoelectrons.

We employ the free-electron model for Ag whose valence electrons fill up a potential well of depth $W=E_F+\Phi$, with $E_F=5.51$ eV referring to the bottom of the potential well as zero energy. $\Phi=1.06$ eV is the Schottky barrier height. Based upon the multiple-step model of photoemission described above, the PQY of photoemission from the base layer can be written (with E being the energy of photoelectrons in the vacuum) as

$$Y_B(h\nu)=K^{-1}(h\nu)(1-R)\int_{E_b-E_v}^{h\nu-E_v+E_c}dE\int_v d^3r[dn(\mathbf{r},h\nu)/dt]P_t^m(\mathbf{r},E)P_{\rm esc}^m(\mathbf{r},E)T_1(E)$$
$$\times P_t^s(\mathbf{r},E)P_{\rm esc}^s(\mathbf{r},E)T_2(E)[(E+E_v)(E+E_v-h\nu)]^{1/2}\Big/\int_A dr^2 J_{\rm ph}(h\nu)\ , \quad (1)$$

where $J_{\rm ph}$ is the incident photon flux of electromagnetic radiation, R the reflectance at the surface, $K=\int_{X_m}^{h\nu+E_f}dE'[E'(E'-h\nu)]^{1/2}$ is the normalization constant with $X_m=\max\{E_f,h\nu\}$, i.e., the larger of the two quantities (E' and E are the energies of photoexcited electrons in the silver particles and in the vacuum, respectively) and $[E'(E'-h\nu)]^{1/2}$ represents the joint density of states[15] for a free-electron system. The remaining terms in the integral correspond to various steps of photoemission to be explained below. Since we are dealing with particle sizes much smaller than the wavelength of the incident wave, we may consider the small-particle suspension as a homogeneous layer with a certain effective dielectric constant or optical absorption

coefficient which is calculated using an extended dynamic effective-medium approximation (DEMA) first proposed by Stroud for granular metal systems[16] and later extended to include coated spheres and the two microstructural units discussed earlier.[3,11,17] For a particle located at a depth z below the interface between the surface and the base layer, the rate of excitation in that specific particle, $dn(\mathbf{r},h\nu)/dt$, can be written as

$$dn(\mathbf{r},h\nu)/dt=\alpha J_{\rm ph}(h\nu)\exp[-\alpha(h\nu)z] , \tag{2}$$

where α is the absorption coefficient given by $\alpha=(2\omega/c)\mathrm{Im}\{\epsilon^{1/2}\}$ and ϵ is the frequency-dependent complex dielectric constant of the effective medium calculated by using the extended dynamic effective-medium theory mentioned above. For a metal particle whose size is on the order of, or less than , the skin depth of the metal at a certain wavelength, it is a good approximation to assume constant excitation rate in the particle. That is to say, although the light intensity gets weaker as it moves farther below the interface, the photoemission mechanisms of each electron taking place in each particle are all the same at a given depth.

After being photoexcited, the electrons move to the Ag-Cs_2O interface in order to escape. Although we have used a free electron model, the photoexcited electrons are subject to inelastic scattering due to, for example, electron-electron, electron-photon, and electron-impurity interactions within the metal particles. This inelastic scattering is contained in the mean free path, $L_m(E)$, of the photoexcited electrons in the metal. For a photoexcited electron at a position $\mathbf{r}$ in a spherical particle centered at $\mathbf{r}=0$, the distance, d, it has to travel to reach the boundary at $\mathbf{r}=\mathbf{R}$ in order to escape is $d(r)=(r^2+R^2-2rR\mu)^{1/2}$, where $\mu=\cos(\mathbf{r}\cdot\mathbf{R})$ and $\mathbf{R}$ is the radius vector pointing towards where the electron hits the boundary. The probability $P_t^{(m)}(\mathbf{r},E)$ that the electron will survive any inelastic scattering in the distance d in the silver metal particle can be written as

$$P_t^m(\mathbf{r},E)=\exp[-d(\mathbf{r})/L_m(E)] , \tag{3}$$

where $L_m(E)$ (Å)$=1000/(e+E_v-E_F)^2$ is the mean free path of the photoexcited electron in a Ag metal particle.[18] The superscript and subscript m's stand for metal.

The transport function, $P_t^m(E)=\langle P_t^m(\mathbf{r}',E)\rangle_{r'}$, i.e., the averaged probability that the electron can reach the particle boundary without inelastic scattering, is therefore

$$P_t^m(E)=(4\pi R^3/3)^{-1}2\pi \times\int_{-1}^{1}d\mu\int_0^R r^2dr\exp[-d(\mathbf{r})/L_m(E)] , \tag{4}$$

which, upon substitution of d into the integral, gives

$$P_t^m(E)=\tfrac{3}{2}(L_m/R)^4\{2(R/L_m)-3+\exp(-2R/L_m)[2(R/L_m)^2+4(R/L_m)+3]\}, \tag{5}$$

where the average $\langle\ \rangle_{r'}$ is carried out through the whole volume of a particle.

When the electron reaches the particle boundary, it will either escape or be scattered away from the boundary. From a quantum mechanical point of view, the scattering of an electron at the particle boundary $r=R$ is elastic, within this free-electron approximation. If the electron does not have enough energy to overcome the energy barrier it will bounce back elastically from the boundary. It is worth mentioning here that the reflection of an electron at the surface is assumed to be diffuse and not specular otherwise the angle of incidences would never change in subsequent reflections. The possible role of impurities in increasing this diffuseness is discussed in a previous publication.[14]

After a reflection from the boundary, the electron will travel a distance, $d'=2R\cos\beta$, to reach the boundary again, β being the angle between the radius pointing towards the reflection point and the direction in which the electron is moving. If the electron in the silver particle has energy $E>W$, but it does not move in a favorable direction so that the vertical energy is smaller than the potential barrier, i.e., $E_\perp=(\hbar K_\perp)^2/2m<W$, the electron will bounce back when it hits the boundary. Provided that the mean free path is long enough so that there is little inelastic scattering before reaching the boundary, the bouncing back and forth of the photoexcited electron in the particle at the boundary may, at some point, bring the electron to a favorable orientation, i.e., more perpendicular to the boundary, for it to escape. The chance for the electron to escape is thus increased because of the multiple reflections in the particle. The probability that a photoexcited electron can survive any inelastic scattering between two reflections averaged throughout the whole spherical particle is[14]

$$P_t^{m'}(E)=L_m(E)/2R\{1-\exp[-2R/L_m(E)]\} . \tag{6}$$

This is the transport function for a photoexcited electron after the first encounter at the particle boundary. The probability $P_n^m(E)$ that an electron will escape after n reflections in a particle, i.e., at the $(n+1)$th encounter at the metal particle boundary, is therefore

$$P_n^m(E)=P_t^m(E)[1-P_{\rm esc}^m(E)]^n[P_t^{m'}(E)]^nP_{\rm esc}^m(E) , \tag{7}$$

where $[1-P_{\rm esc}^m(E)]^n[P_t^{m'}(E)]^n$ gives the probability for a photoexcited electron to reflect n times with neither escape nor inelastic scattering. $P_{\rm esc}^m(E)$ is the escape function for the photoexcited electron to penetrate the Ag-Cs_2O barrier. It is the probability for an electron to possess vertical kinetic energy greater than the potential barrier and to escape. $P_{\rm esc}^m(E)=\langle P_{\rm esc}^m(\mathbf{r},E)\rangle_{\rm r}$ where $P_{\rm esc}^m(\mathbf{r},E)$ imposes on the photoexcited electron the condition that only those electrons with vertical energy greater than the potential barrier can escape. Obviously,

$$P_{\rm esc}^m(\mathbf{r},E)=\Theta(E+E_v-W)\Theta(\theta_c-\theta) , \tag{8}$$

where $\Theta(x)$ is Heaviside's unit step function and θ_c is the critical angle of the escape cone.

It can now be shown that

$$P_{\rm esc}^m(E)=\tfrac{1}{2}[1-(W/E+E_v)^{1/2}]\Theta(E+E_v-W) , \tag{9}$$

where E_v is the vacuum level at the Cs_2O surface, $E+E_v$ is the energy of the photoexcited electron in the silver particle and $W(=E_b)$ is the potential barrier the electron has to overcome in order to penetrate from a silver particle into the cesium oxide. This escape function gives the probability for a photoexcited electron to move in a favorable direction so that the vertical energy of the electron is greater than the potential barrier and the electron can penetrate it. From (7), the total probability for a photoexcited electron to penetrate can be written as

$$\sum_{n=0}^{\infty} P_n^m(E)=P_{\rm esc}^m(E)P_t^m(E)/\{1-[1-P_{\rm esc}^m(E)]P_t^{m'}(E)\} . \tag{10}$$

Note that a geometric enhancement factor $\gamma=1/\{1-[1-P_{\rm esc}^m(E)]P_t^{m'}(E)\}$ occurs because of multiple internal reflection. The γ factor can be as high as 20 near the spectral response cutoff region of the S-1 photocathode. As the Ag particle size decreases, this geometric factor becomes even more pronounced. This will be shown later in Sec. IV.

Upon penetrating into the cesium oxide from the silver particle, the photoexcited electrons will have the transmission coefficient with image force included given by

$$T_1(E)=\{1+E_b^4/[16E_H(E+E_v)^3]\}^{-1} , \tag{11}$$

where E, again, is the energy of the photoelectron in the vacuum. E_b $(=W)$ and E_v are, respectively, the potential barrier height at the silver-cesium oxide interface and the vacuum level of the Cs_2O as indicated in Fig. 1(b). Note that we have referred to the bottom of the conduction band of the silver metal as the zero energy level. Only those electrons with energy greater than E_b are transmitted. In calculating the transmission coefficient at the Schottky barrier, we do not employ the WKB method, in which the width of Schottky barrier has to be involved, in order not to introduce more physical complications. For those photoexcited electrons with energy greater than E_b, only those with vertical energy greater than E_b will penetrate. The escape (penetration) probability obtained from Eq. (9) is

$$P_{\rm esc}^m(E)=\tfrac{1}{2}\{1-[E_b/(E+E_v)]^{1/2}\}\Theta(E+E_v-E_b) . \tag{12}$$

After penetrating into the Cs_2O, the electron now moves to the cesium oxide-vacuum interface (step 4). The probability for the electron to survive any inelastic scattering is

$$P_t^s(\mathbf{r},E)=\exp[-|\mathbf{r}-\mathbf{r}_0|/L_s(E)] , \tag{13}$$

where $\mathbf{r}_0$ is the location where the electron was photoexcited and L_s, the mean free path of the electron in the Cs_2O, is hundreds of angstroms.[2] For electrons in cesium oxide with kinetic energy greater than the electron affinity of the cesium oxide, only those with vertical energies greater than the electron affinity of the cesium oxide will escape. The escape function can be written as

$$P_{\rm esc}^s(E)=\tfrac{1}{2}[1-(\chi/E)^{1/2}] , \tag{14}$$

where χ is the electron affinity of the Cs_2O, E is the energy of the photoexcited electron in the cesium oxide and the superscript s stands for the semiconductor, Cs_2O. Adhering to the convention that E is the photoelectron energy in the vacuum, we may rewrite (14) as,

$$P_{\rm esc}^s(E)=\tfrac{1}{2}\{1-[(E_v-E_c)/(E+E_v-E_c)]^{1/2}\} , \tag{15}$$

where E_c is the bottom of the conduction band of Cs_2O. Finally, for those electrons that are able to escape, a potential step from E_c to E_v will be perceived which leads to a transmission coefficient $T_2(E)$, which may be written as

$$T_2(E)=\{1+(E_v-E_c)^4/[16E_H(E+E_v-E_c)^3]\}^{-1} . \tag{16}$$

Using (16), we readily obtain for $Y_B(h\nu)$

$$\begin{aligned} Y_B(h\nu)=K^{-1}(h\nu)(1-R)\int_{E_b-E_v}^{h\nu-E_v+E_c} dE\,[(E+E_v)(E+E_v-h\nu)]^{1/2}[\alpha L_s/(1+\alpha L_s)] \\ \times\{1-\exp[-(\alpha+1/L_s)]H_b\}T_1(E)P_{\rm esc}^m(E)P_t^m(E) \\ \times T_2(E)P_{\rm esc}^s(E)/\{1-[1-P_{\rm esc}^m(E)]P_t^{m'}(E)\} , \end{aligned} \tag{17}$$

where H_b is the base layer thickness. Note that the integration limits in (17) have been set in such a way that only electrons with energy greater than the potential barrier $W=E_b$ are counted. This takes care of the condition imposed earlier saying that only those electrons with $E>W=E_b$ are transmitted. This expression is the photoelectric yield for the base layer of the S-1 photocathode.

Now we consider the surface layer where silver particles are coated with $Cs_{11}O_3$ and are suspended in the vacuum with $\epsilon=1$. The coating of $Cs_{11}O_3$ serves only to lower the work function of the silver from 4.9 eV to about 1.1 eV, but does not contribute to the dielectric constant of the particles since it is assumed very thin.[3] The photoemission process thus reduces to (1) photoexcitation, (2) transport of electrons to the particle boundaries, and (3) elastic multiple scattering transmission. To obtain the PQY of this layer, we can still use (17) in which several parameters require corrections. We do this by replacing H_b, the thickness of the base layer, with H_s, the thickness of the surface layer. Meanwhile, since the Cs_2O has to be replaced by vacuum, we can put $L_s(E)$ as infinite and $T_2(E)=1$. The vacuum level E_v also has

to be replaced with E_b. We therefore have

$$T_1(E)=\{1+E_b^4/[16E_H(E+E_b)^3]\}^{-1} . \tag{18}$$

Furthermore, the integration limits start from zero energy to $h\nu-\Phi=h\nu-(E_b-E_F)$, i.e., the extreme photoelectron energies. The PQY due to the surface layer can thus be written as

$$Y_S=K^{-1}(h\nu)(1-R)[1-\exp(-\alpha H_s)]\int_0^{h\nu-E_b+E_F} dE\,[E+E_b)(E+E_b-h\nu)]^{1/2} \times T_1(E)P_t^m(E)P_{\rm esc}^m(E)/\{1-[1-P_{\rm esc}^m(E)]P_t^{m'}(E)\} . \tag{19}$$

The total PQY is thus

$$Y(h\nu)=Y_s(h\nu)+Y_B(h\nu)T(h\nu)(1-P^{2/3}) , \tag{20}$$

where $T(h\nu)$ is the transmittance of the incident electromagnetic wave at the surface-base layer interface. P is the volume fraction of the silver particles in the surface layer. The factor $1-P^{2/3}$ gives the effective area for the electrons in the base layer to get into the vacuum without being screened by the silver particles on the top. Equation (20) is the equation we employed to calculate the quantum yield of the S-1 photocathode. What remains to be determined are the optical absorption coefficients of each layer. As mentioned earlier in the Introduction, we use the extended DEMA to calculate the effective dielectric constant of the heterogeneous system to obtain the absorption coefficients. This has been described elsewhere[16,17] and will not be repeated here. We will simply give the principles of that calculation and then give numerical results on the optical properties of the S-1 photocathode in the following section.

III. OPTICAL PROPERTIES OF THE S-1 PHOTOCATHODE

Although the properties of the S-1 have been studied in great detail since its discovery in 1929,[1] few studies have looked at the relationship between its microstructure and optoelectronic properties. Notable exceptions include the work by Asao[19] who observed that the absorption peak of the Ag film used in the S-1 moved to longer wavelengths with increasing thickness and that of Wu[12,13] whose "equivalent particle" approach suggested the importance of the smaller Ag particles in determining the photoemissive properties of the S-1. Sommer[2] also observed that the optical absorption of the S-1 was somewhat insensitive to the silver deposited during the "additional silvering" process and although it did increase the PQY it sometimes reduced the long wavelength threshold. Our own recent efforts on this surface have emphasized the microstructure and its relation to optoelectronic properties and this section is an extension of that work.

Here we use the extended DEMA mentioned previously to calculate the optical properties of the S-1. In this case multiple reflections of light at the interface between various layers [vacuum ($n=1$)/ surface layer / base layer / glass substrate ($n=1.5$), where n represents the index of refraction] is accounted for in this calculation.[20] Also, without losing insight into the physics of photoemission of the S-1, we have assumed normal incidence of radiation which, unlike the p-polarized wave at oblique incidence, cannot provoke collective motion of electrons (plasma resonance-longitudinal mode) in the films of random heterostructures. The film is transparent to the incident wave at the plasma frequency as will be shown later.

The frequency-dependent dielectric constants of bulk silver for the S-1 and bulk gold and copper for other calculations are taken from the work by Johnson and Christy.[21] Because of the scattering of electrons at the metal particle boundaries, the dielectric constant of a single spherical metal particle can be obtained by modifying the scattering time (mean free collision time) of the electrons in the metal. The total dielectric constant can be separated into free- and bound-electron parts, i.e., $\epsilon_j=\epsilon_j^f+\epsilon_j^b$, where j indicates either bulk or particulate metal. Using the Drude model for metals,[22] one can write

$$\epsilon_{\rm bulk}^f=1-\omega_p^2/[\omega(\omega+1/\tau_{\rm bulk})] \tag{21}$$

and

$$\epsilon_{\rm particle}^f=1-\omega_p^2/[\omega(\omega+i/\tau_{\rm particle})] , \tag{22}$$

where $\omega_p=4\pi Ne^2/m_0$ is the free-electron plasma frequency, N is the density of the conduction electrons, and m_0 is their effective mass in the metal. Assuming that the bound electron part remains the same for both cases, the dielectric constant for a spherical metal particle can be written as follows:

$$\epsilon_{\rm particle}=\epsilon_{\rm bulk}-\epsilon_{\rm bulk}^f+\epsilon_{\rm particle}^f . \tag{23}$$

The scattering rate in the particle, $1/\tau_{\rm particle}$, is the sum of the scattering rates at the boundary and inside the particle. The bulk silver scattering time is $\tau_{\rm bulk}=3.1\times10^{-14}$ sec given also by Johnson and Christy.[21] This value is not too far from 1.44×10^{-14} sec given by Hodgson.[23] The total scattering time $\tau_{\rm particle}$, in the silver particle, is hence given by

$$1/\tau_{\rm particle}=1/\tau_{\rm bulk}+V_f/D , \tag{24}$$

where V_f is the Fermi velocity of electrons in the silver metal taken as 1.39×10^3 cm/sec and D is the diameter of the spherical particle.

Having obtained the dielectric constant for a single spherical particle, we can use the extended DEMA (Refs. 16 and 17) to calculate the effective dielectric constant of a collection of small metal particles with various microstructures. As mentioned previously, we have to consider

two types of microstructural units for the heterostructural systems we are dealing with in this paper. From electron microscopic studies of the S-1 photocathode,[12,13] it has been shown that silver particles exist both in the forms of isolated islands and aggregated particles. The isolated silver particles can be modeled as metal particle coated with shells of semiconductor (cesium oxide) which are called the first units. The aggregated silver particles, on the other hand, can be modeled as semiconductor particles coated with metal shells which are called the second units.

Suppose there is an ensemble of particles in which the jth spherical particle with dielectric constant x_j^k is surrounded by a spherical shell of material with dielectric constant y_j^k. Furthermore, this ensemble of particles has the two units ($k=1$ and 2) of coated spheres, one with the metal coated by the semiconductor and the other with the semiconductor coated by metal, which makes up an self-consistent effective medium with dielectric constant ϵ_{eff}. The effective medium consists of the rest of the material in which the particle under consideration is embedded. Since the particle size is much smaller than the wavelength and hence the electromagnetic wave cannot resolve the individual particles, the effective medium can be looked upon as homogeneous and, as a result, ϵ_{eff} should be constant as a function of spatial position. The forward scattering amplitude $S_k(0)$ for the plane electromagnetic wave scattered from such a collection of individual types of coated spheres indexed with k, where $k=1$ for the first unit and $k=2$ for the second unit, can be written in the form[24–26]

$$S_k(0)=\tfrac{1}{2}\sum_j\sum_n(2n+1)\times\iint dr\,dR\,\rho_k(R)[a_n(r,R,x_j^k,y_j^k\epsilon_{\text{eff}})+b_n(r,R,x_j^k,y_j^k,\epsilon_{\text{eff}})]\ , \tag{25}$$

where $\rho_k(R)$ is the size distribution of the kth microstructural unit of coated spheres with the inner sphere of radius r and the outer sphere of radius R. The functionals a_n and b_n are, respectively, the electric and magnetic multipole contributions to the scattered fields due to the small-particle scattering which are equivalent to the partial-wave scattering amplitudes[24,25,27] for the scattering of electromagnetic waves from a coated sphere. The double sums run over all multipoles (n) and all particles (j). For the jth particle of the first unit microstructure, $x_j^1=\epsilon_m$ is the dielectric constant of the metal particle (the inner sphere of radius r) given by Eq. (23) and $y_j^1=\epsilon_M$ (the spherical shell of outer radius R) is the dielectric constant of the host (semiconductor) matrix assumed constant in the range of frequency concerned. If the jth particle is of the second microstructure, $x_j=\epsilon_M$ (the inner sphere of radius r), $y_j^2=\epsilon_m$ (the spherical shell of outer radius R). Under the condition that the particle size is much smaller than the wavelength of the incoming electromagnetic radiation and that the dielectric constants of the components are not too large, it was found[25,26] that only the dipole terms a_1 and b_1 are important. Suppose that the fraction of the first and the second microstructural unit are f_1 and f_2, respectively, where $f_1+f_2=1$, the DEMA leads to the conclusion that the forward scattering amplitude of the scattered wave from an ensemble of two types of coated small particles, with particle size much smaller than the wavelength, should vanish on the average, namely,

$$f_1S_1(0)+f_2S_2(0)=0\ . \tag{26}$$

Knowing the particle size $D=2r$, the volume fraction of the metal particle $p=(r/R)^3$, the fraction of the second unit f_2 and the dielectric constants of Ag and the semiconductor, we can employ Eqs. (25) and (26) to solve for ϵ_{eff}. Having the dielectric constant, we can obtain the optical properties of the effective medium.

Consider first the optical properties of the surface layer of the S-1 photocathode. As mentioned earlier in Sec. II, it is an 100-Å thick layer of $Cs_{11}O_3$-coated Ag particles suspended in a matrix whose dielectric constant ϵ is 1. The Ag particle size is 50 Å and the Ag volume fraction is 50% in which 2% are the aggregated Ag particles. This surface layer resides on a 300-Å thick base layer of $Cs_{11}O_3$-coated Ag particles embedded in cesium oxide ($\epsilon=4$). In the base layer, the Ag particle volume fraction is again 50% and the particle size ranges from ≈ 100 Å to ≈ 1500 Å. The variation of particle size obeys the γ-type distribution function with mode radius $R_m=700$ Å.[27] The γ-type size distribution function is $\rho(R)=R^{\alpha}\exp(-\alpha R/R_m)$. Specifically in this calculation, α is a distribution factor taken as ≈ 4 in the size distribution for the base layer just mentioned. These two layers together on a glass substrate ($n\approx 1.5$) make up the S-1 photocathode.

Figures 2–4 show the optical absorption coefficient and the corresponding transmittance, reflectance, absorptance, and optical conductivity of the surface layer. In Fig. 2 for the surface layer, we see that the absorption coefficient of the bulk silver is fairly constant from the visible into the infrared. The high absorption coefficient corresponds to high reflectivity in this wavelength range, i.e., the free electrons contribute to the scattering rather than the absorption of the electromagnetic wave. For the Ag particles at 3.8 eV (≈ 0.33 μm), there is a dip which is due to the plasma oscillations as will become clear later on. Below 0.33 μm (or roughly above 4 eV), interband transitions come into play[22] due to the Ag 4d electrons at 4 eV below the Fermi energy. For the particulate Ag system, the absorption coefficient is lower than that of the bulk Ag. The reflectivity of the S-1 surface is considerably lower both in the visible and infrared than that of the bulk Ag as shown in Fig. 3, where we include the T and R of both particulate and bulk (continuous) Ag films of the same mass thickness (100 Å for the former and 50 Å for the latter) for comparison. However, as shown in Fig. 4, the absorptance of the S-1 surface layer is higher than the bulk Ag beyond 0.33 μm. In Fig. 4 at ≈ 0.41 μm, there is an enhanced absorption due to the bound nature of the free electrons in the Ag particles.

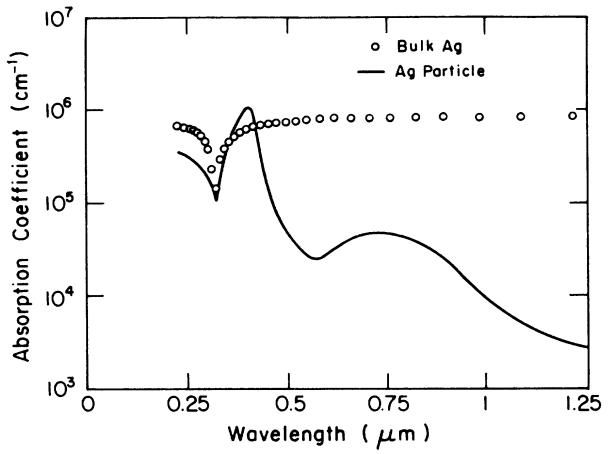

FIG. 2. Dynamic effective-medium calculation (DEMA) of optical absorption coefficient of a surface layer of Ag-particle suspension compared to the bulk Ag (or continuous film). $d = 50$-Å diameter Ag-particles, $H = 100$-Å thick film, $p = 50\%$ volume fraction of Ag, $f_2 = 2\%$ volume fraction of second unit, and $\epsilon_m = 1$ (dielectric constant of host matrix).

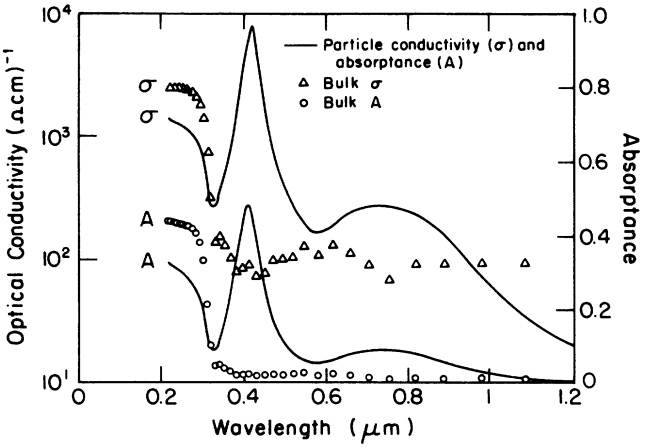

FIG. 4. Dynamic effective-medium calculation of absorptance and optical conductivity corresponding to Figs. 2 and 3.

This peak is called the dielectric anomaly or the anomalous dispersion which is due to the isolated Ag particles. The optical conductivity of the Ag particles is also larger than the bulk Ag from the visible up to 1 μm. At longer wavelengths, the bulk has high metallic conductivity while the Ag particles tend towards an insulator in the dc limit, as shown in Fig. 5.

The anomalous dispersion is a well-known physical phenomenon in many intervals of the entire electromagnetic spectrum of the electromagnetic-radiation–solid interactions. At those certain frequency intervals, the index of refraction or the real part of the dielectric constant decreases as the frequency increases, contrary to the normal dispersion. The ionic lattice vibrations in the infrared is one example of the commonly known anomalous dispersions. When this dispersion occurs, there is a peak in the imaginary part of the dielectric constant accompanied by an oscillatory real part of the dielectric constant. This phenomenon can be understood using the Lorentzian oscillator model which involves a scattering time τ and a natural frequency ω_0 corresponding to a restoring force. The electronic contribution to the anomalous dispersion can also be treated in a similar fashion. Although free electrons do not absorb the visible or infrared radiation due to a lack of restoring force on them, a restoring force can be created if they become bounded by particle boundaries on which surface charges are accumulated at the excitation of light. (Note that the Drude

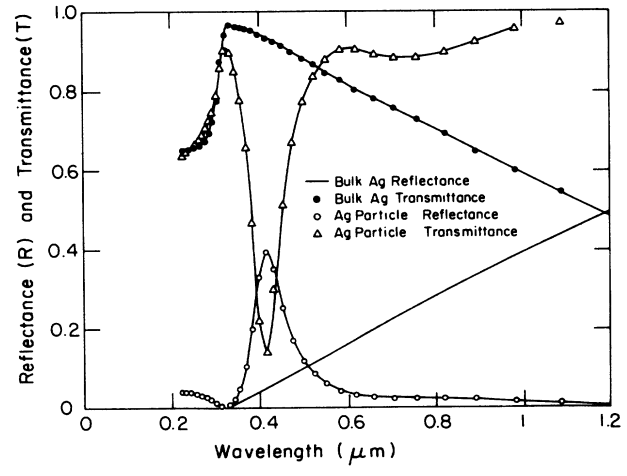

FIG. 3. Dynamic effective-medium calculation of R and T for a Ag-particle suspension with the same parameter of Fig. 2 as compared with a continuous (bulk) film of Ag with equal mass thickness, i.e., 100 Å ($p = 50\%$, discontinuous film) vs 50 Å ($p = 1$, continuous film).

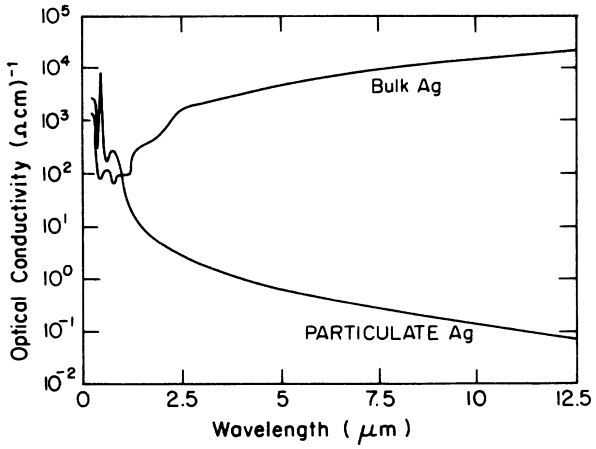

FIG. 5. Dynamic effective-medium calculation of optical conductivity variations for bulk and particulate Ag films with parameters from Fig. 3.

model of free-electron metals is simply the Lorentzian model with zero restoring force.)

Figure 6 shows the real (ϵ_1) and imaginary (ϵ_2) parts of the dielectric constant and the quality factor of the surface layer of the S-1 photocathode with no second microstructural unit and hence no absorption peak at ≈ 0.8 μm. The quality factor $Q = \epsilon_1/\epsilon_2 = 1/\tan\delta$ is proportional to the ratio of energy stored versus the averaged energy loss per period of oscillation and δ is the loss angle. We can readily identify the oscillatory characteristic of ϵ_1 for an anomalous dispersion at $\lambda = 0.41$ μm. Note that when photoabsorption occurs at this wavelength, the quality factor drops. This corresponds to a resonance, not occurring in the bulk Ag, due to the bound free electrons in silver particles. The photon energy is absorbed to excite electrons in the Ag particles. In Fig. 7, we put in 2% of the second microstructural units. We see an additional resonance at $\lambda \approx 0.8$ μm, corresponding to the near infrared response of the S-1 photocathode. In Figs. 6 and 7 note the minima in quality factors and the similar oscillatory features of anomalous dispersion at the two distinct resonance wavelengths 0.4 and 0.8 μm. The absorption at ≈ 0.8 μm is thus a surface mode resonance, a cavity resonance due to the second microstructural unit (aggregated Ag particles) as discussed in Refs. 9 and 26. The peak near 0.41 μm is due to isolated silver particles. To make the second unit contribution to the resonance clearer, Fig. 8 for Ag with parameters for Figs. 2–4 taken from Ref. 11 demonstrates that as the fraction of the second unit increases from 0 to 0.2 the absorption in the infrared also goes up from ≈ 0 to $\approx 10\%$. This absorption peak due to the second unit can be called the second unit dielectric anomaly.

In parallel with the Ag-particle heterostructural system, Au and Cu also show similar behavior due to the aggregation of the small particles. Figures 9 and 10 (from Ref. 26) show the second unit effects on the optical absorptions of Au and Cu systems, respectively. This calculation predicts a dielectric anomaly at ≈ 2.3 eV (0.53 μm) for the Au-particle system due to the isolated Au particles, close to the value measured by Yamaguchi *et al.*[28] which is ≈ 2.2 eV (0.56 μm). As for Cu, the dielectric anomaly occurs at ≈ 2.2 eV (0.56 μm). Note that this peak has been somewhat obscured by the interband transition which takes place at about 2 eV for Cu. Nevertheless, the enhanced photoabsorptions in the infrared due to the second microstructural units are evident. The absorptions peak at ≈ 0.8 μm for both Au and Cu whose particle volume fractions are 40%. At the same volume fraction, the second unit peak of Ag occurs at ≈ 0.6 μm as shown in Fig. 11 for an 100-Å thick layer of the singly sized Ag-particle suspension with diameter 50 Å and 2% aggregation. In this figure, we see that, at constant fraction of the second unit, the increasing volume fraction of

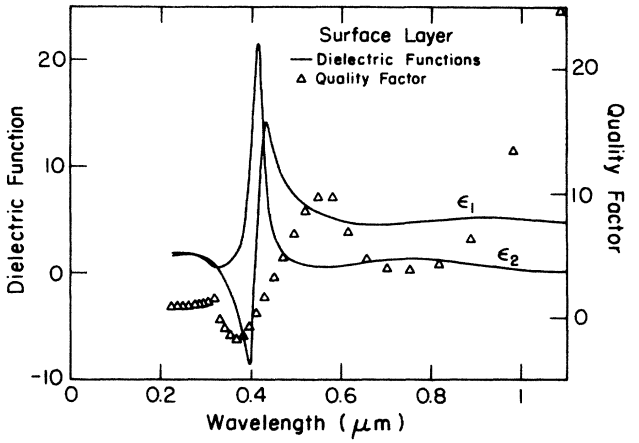

FIG. 7. Same as Fig. 6, except that 2% volume fraction of the second unit exists.

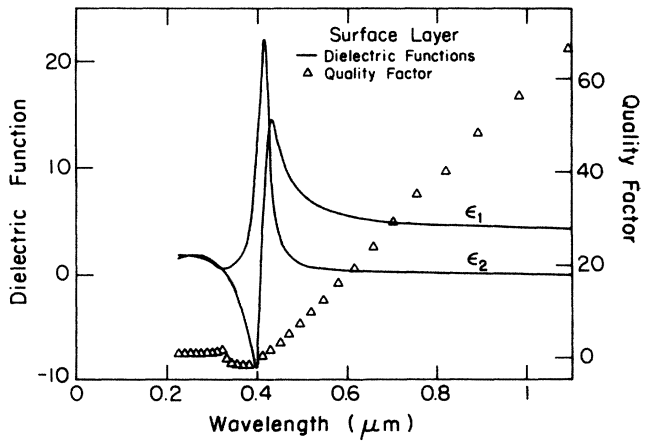

FIG. 6. Dynamic effective-medium calculation of the Q factor, real and imaginary part of the complex effective dielectric constant corresponding to Figs. 2–4, except that there is no second unit included in this layer.

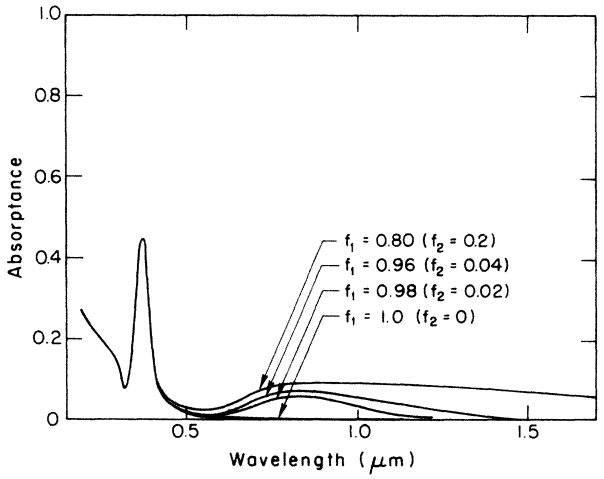

FIG. 8. Dynamic effective-medium calculation of the second unit effect on the absorptance of the S-1 surface with microstructural parameters $d = 50$ Å, $H = 100$ Å, $p = 50\%$, $f_2 = 0$, 2, 4, 20%, and $\epsilon_M = 1$ (from Ref. 26).

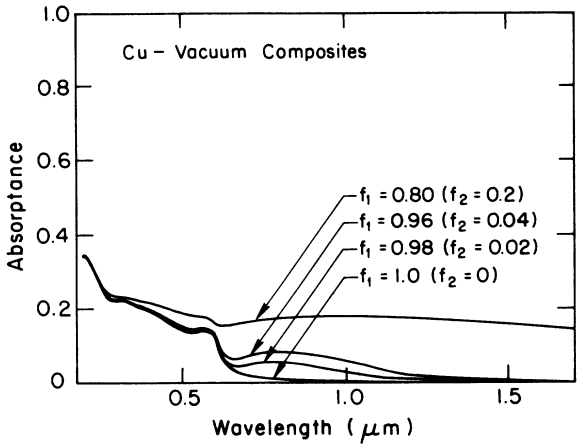

FIG. 9. Dynamic effective-medium calculation of absorption of Cu-particle suspension. $d=50$ Å, $H=1000$ Å, $p=40\%$, $f_2=0$, 2, 4, 20%, and $\epsilon_M=1$.
Note that the increasing absorption above 2 eV is due to interband transitions (from Ref. 26).

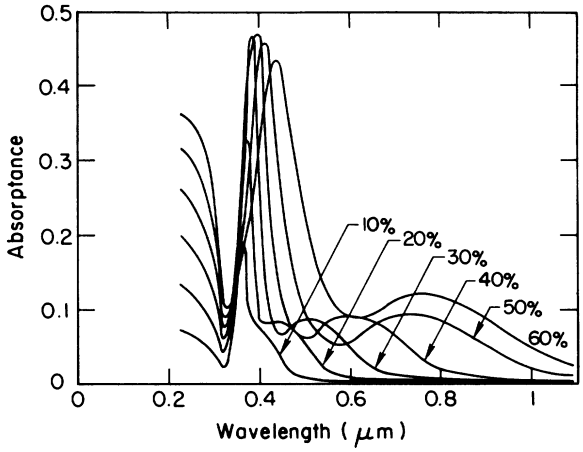

FIG. 11. Dynamic effective-medium calculation of Ag volume-fraction effects on the optical absorption of the S-1 surface. $d=50$ Å, $H=100$ Å, $p=10$, 20, 30, 40, 50, and 60%, $f_2=2\%$, and $\epsilon_M=1$.

silver particles shifts the optical absorption toward the infrared. Meanwhile, the peaks broaden and the peak intensities change with increasing Ag volume fractions, as listed in Table I.

From Table I and Fig. 11, we see that when the Ag volume fraction is low the absorption due to the isolated Ag particles (first unit) is also low. As the volume fraction increases to above 40%, the scattering time becomes smaller corresponding to line shape broadening. This is understandable since as the number of Ag particles increases, the inter-Ag-particle interactions become more prominent and the scattering rate (damping) of electrons in the particle thus increases. Note that according to Eq. (24), the scattering time of a single Ag particle 50 Å in diameter is 3.22×10^{-15} sec. The scattering rate for a collection of similar small particles has thus been increased by a factor of 2–4 depending on the volume fraction, reflecting the electron-electron interactions between Ag particles. The peak intensity increases while the peak width (and hence the scattering time) remains pretty much constant as a function of the Ag volume fraction from 10% to 40%. This seems natural because more Ag particles should contribute to more photoabsorption if the damping of the bounded free electrons due to the inter-Ag-particle interactions is not important at low Ag concentration. Above 40%, the peak intensity decreases while the peak width (and hence the scattering rate) increases as the Ag volume fraction increases. This can be understood using the Lorentzian oscillator model for forced oscillations. At these higher concentrations, the optical absorption may not be a drastic function of concentration. However, since the resonance peak intensity is proportional to τ/ω_0,[29] the intensity should weaken as the peak broadens while it should get stronger as the resonance has a red shift.

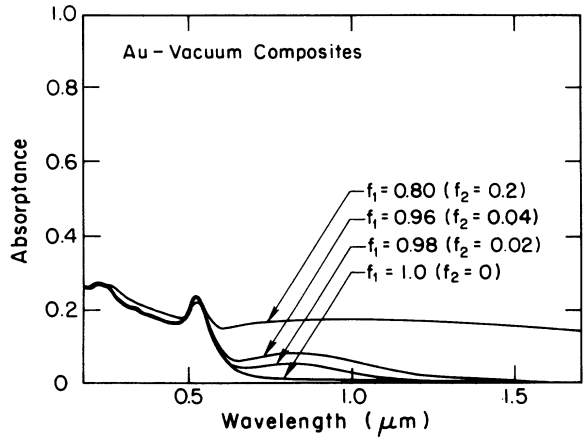

FIG. 10. Dynamic effective-medium calculation of absorption of Au-particle suspension. $d=50$ Å, $H=1000$ Å, $p=40\%$, $f_2=0$, 2, 4, 20%, and $\epsilon_M=1$. The increasing absorption above 2 eV is due to p interband transitions (from Ref. 26).

The reason for the red shift is the increase in the effective refraction index n_{eff} where $(n_{\text{eff}}+ik_{\text{eff}})^2=(\epsilon_1)_{\text{eff}}+i(\epsilon_2)_{\text{eff}}$. Similar to the effect of increasing polarizability of metal particles by selecting an embedding dielectric (or semiconductor) matrix with larger dielectric constant ϵ_m, the increasing volume fraction p creates a more polarizable environment due to the larger refractive index n_{eff}. This will be further discussed later on. The respective values of n_{eff} and k_{eff} at the resonance wavelengths for the two units of microstructure are also listed in Table I. The point is that these two factors (lifetime τ and resonance frequency ω_0), together with the fact that the increasing particle volume fraction increases the optical cross section, can account for the overall variations of peak intensities and the line shapes near 0.41 and 0.8 μm in Fig. 11. As shown in the same figure for the second microstructural unit near 0.8 μm, there are also red shifts and line broadenings as a function of increasing volume fraction. These peak values are listed in Table I. Precise

TABLE I. Concentration effects: A 100-Å thick layer of 50-Å diameter Ag particles in vacuum.

Volume fraction P (%)	10	20	30	40	50	60
First unit peak position ω_0 (μm)	0.35	0.37	0.37	0.38	0.41	0.43
n_{eff} at first unit peak position	1.0	1.12	1.23	2.15	2.58	3.15
k_{eff} at first unit peak position	0.67	1.54	1.89	3.71	4.19	4.65
First unit peak intensity (%)	19	40	45	47	46	43
First unit FWHM (eV) $\Delta\omega=1/\tau$	0.4	0.4	0.4	0.5	0.6	0.9
Scattering time τ ($\times 10^{-15}$ sec)	1.65	1.65	1.65	1.32	1.10	0.73
2nd unit peak position (μm)	x[a]	0.45	0.52	0.62	0.76	0.98
2nd unit peak intensity (%)	x[a]	8.1	8.6	8.9	9.0	11.9
n_{eff} at 2nd unit peak position	x[a]	1.51	1.73	1.91	2.15	2.54
k_{eff} at 2nd unit peak position	x[a]	0.21	0.23	0.26	0.30	0.31

[a]Not observed.

linewidths are not easy to extract from this figure at 0.8 μm due to the weak peak intensities and therefore no attempt is made here to explain the intensity change as a function of Ag volume fraction. Similar host matrix refraction index effects have also been observed for alkali-metal particles embedded in alkali-halide matrices.[30]

Before going any further into other microstructural effects, we look at the plasma oscillation of a small Ag particle system. From Figs. 12(a) and 12(b), we see that the real part of the complex dielectric constant vanishes while the imaginary part is very small (or close to zero) at about 3.74 eV (3315 Å). The optical energy loss function[31,32] $-\text{Im}\{1/\epsilon\}=\epsilon_2/(\epsilon_1^2+\epsilon_2^2)$ peaks at the same energy. This function should show a δ-function type behavior at the volume plasma frequency.[15,31] It occurs at ≈ 3.9 eV (3200 Å) for bulk Ag. We thus see that the plasma oscillation for the small Ag particles takes place at a lower frequency than bulk silver. The minima at ≈ 3.8 eV in the optical absorption curve as well as the spectral response (quantum yield) curve of the small Ag particle system (S-1 photocathode) are due to the plasmon losses. At the plasma frequency, the transmittance should show a maximum for normal incident wave while the reflectance a minimum. This is shown in Fig. 3. For surface plasma oscillation, it is believed that the surface optical loss function, $-\text{Im}\{1/(\epsilon+1)\}=\epsilon_2/[(\epsilon_1+1)^2+\epsilon_2^2]$, should also show a δ-function type behavior at the surface plasma frequency.[15] This occurs at ≈ 3.62 eV (3425 Å) for both bulk Ag and Ag-particle suspension. From Fig. 3, it is found that the transmittance maximum and reflectance minimum occur at ≈ 3.74 eV for the S-1 surface. This leads us to believe that volume plasmon loss in the photoelectric quantum yield, as will be shown later in Sec. IV, could be responsible for the minimum in the spectral response of the S-1 at 3.8 eV.

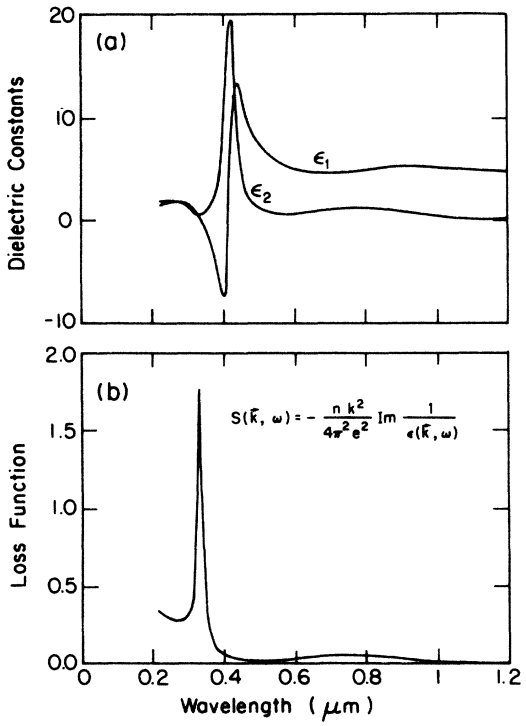

FIG. 12. Comparison of the dielectric functions and the optical loss function of the S-1 surface layer using DEMA.

We now consider the particle-size effects on the optical properties. Figure 13(a) gives a three-dimensional (3D) plot of the optical absorption of the S-1 surface whose Ag particle size ranges from 20 to 90 Å. It is seen that the second unit peaks are less conspicuous at smaller particle sizes for the same amount of the second unit. In other words, at a bigger particle size, the optical absorption peak around 0.8 μm sharpens for constant fraction of particle aggregations. This is reasonable for the scattering rate is higher for smaller particles which leads to the broadened line shape. The size effect on the line shape broadening also comes up in the first unit absorption peak. This peak at 0.4 μm broadens as the particle size decreases, though it also intensifies. The weakening of the first unit peak at increasing particle size can be explained as follows.

As discussed previously, dielectric anomaly is characteristic of the bounded free electrons in the small metal particle. When particles become bigger the free electrons start losing their bound nature which leads to the lower scattering rate due to the particle boundaries. The resonance peak width therefore decreases. In the mean time,

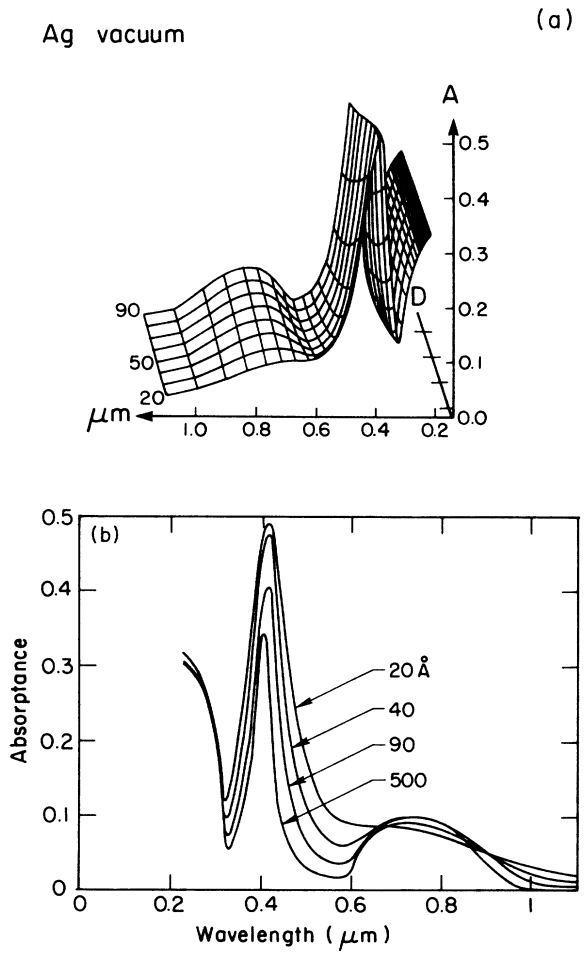

FIG. 13. (a) and (b) Dynamic effective-medium calculation of Ag-particle-size effect on the S-1 surface layer. $d=20$–90 Å in diameter, $H=100$ Å, $p=50\%$, $f_2=2\%$, and $\epsilon_M=1$.

the peak intensity drops because, at constant volume fraction of the silver, the number density of the Ag particles drops at increasing particle size. The contribution of bounded free electrons to the resonance is thus reduced, giving rise to the lower peak intensity. To get a clearer picture of the change of the line shape due to particle size effects, we show in Fig. 13(b) a plot revealing the size effects. These results are listed in Table II.

Now, we consider the optical properties of the whole S-1 photocathode with a surface layer residing on a base layer. It is well known that the absorption curve is qualitatively different from the photoelectric quantum yield (PQY) curve for the S-1 photocathode.[2] Because of the inelastic scattering of the photoelectrons in the material, the surface layer is dominant in producing the PQY. The optical absorption, on the other hand, is due to both the surface and the base layers, although a large fraction of the photoexcited electrons in the base layer may not be able to escape into the vacuum and be collected as photoelectrons. In Fig. 14, taking the multiple reflection of light into account, we show the absorptance of a multilayered structure of vacuum/surface layer/base layer/glass substrate. Again, the surface layer is 100-Å thick with Ag-particle 50 Å in diameter, 50% volume fraction and 2% of aggregation. This ensemble of Ag particles is embedded in a host medium of unit dielectric constant. The base layer is 300-Å thick with 50% volume fraction and 30% of aggregation of Ag particles embedded in cesium oxide of dielectric constant 4. The particle size in the base layer is larger than the surface layer and ranges from ≈ 100 Å to ≈ 1000 Å.[12,13] As mentioned previously, the particle-size distribution in this layer follows the γ-type distribution function with mode radius 700 Å and α factor ≈ 4. The absorptance curve of the composite agrees quite well with the experimental results shown in Sommer's book.[2] Figure 14 also contains the absorptance of individual layers for comparison. From the lineshape and peak positions, we can infer that the spectral response of the S-1 photocathode must be due to the surface layer while the optical absorption is dominated by the base layer. This agrees with Sommer's interpretation of the optical absorption behavior of the Ag-Cs_2O composite in the visible and infrared as due to the constant photoabsorption of silver particles.

So far, we have shown the microstructural effects on the optical properties of the S-1. The structural parameters are the Ag-particle size and its distribution, the volume fraction, the percentage of aggregation and the embedding host matrix. Based upon these calculations, we can now calculate the PQY of the S-1 and make comparisons with experimental results.

IV. NUMERICAL RESULTS OF PHOTOELECTRIC QUANTUM YIELDS

In this section, we will present the numerical results of the PQY of the S-1 photocathode based on the multiple-

TABLE II. Size effects: A 100-Å thick layer of 50% Ag particles in vacuum with 2% second unit.

Particle diameter (Å)	20	40	90	500
First unit peak position ω_0 (μm)	0.41	0.41	0.41	0.40
First unit peak intensity (%)	49	48	40	30
First unit FWHM (eV) $\Delta\omega=1/\tau$	0.9	0.7	0.5	0.4
Scattering time τ ($\times 10^{-15}$ sec)	0.73	0.94	1.32	1.65
2nd unit peak position (μm)	x[a]	0.70	0.80	0.80
2nd unit peak intensity (%)	x[a]	8.9	9.5	9.8

[a]Not observed.

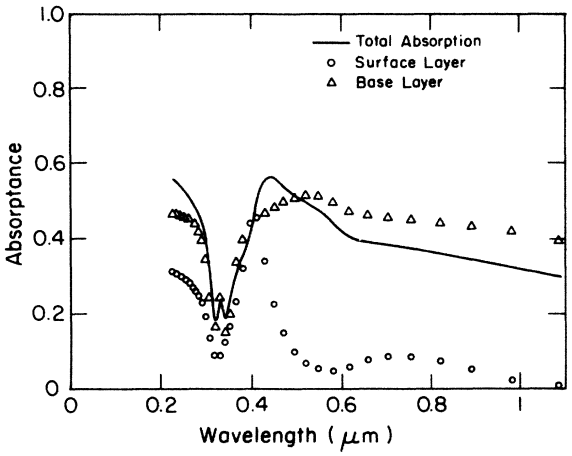

FIG. 14. Dynamic effective-medium calculation of the optical absorption of the S-1 photocathode, included also are the individual layers. $D=50$ Å, $H=100$ Å, $p=50\%$, $f_2=2\%$, $\epsilon_M=1$ for surface layer. $Dm=2Rm=700$ Å, $H=300$ Å, $p=50\%$, $f_2=30\%$, $\epsilon_M=1$ for base layer. D ranges from $\approx 100-1000$ Å corresponding to $\alpha=4$ in the γ distribution.

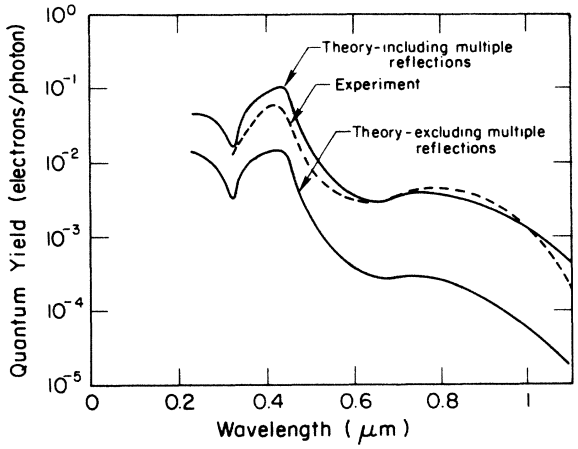

FIG. 15. The geometric enhancement due to the multiple reflections of electrons in the Ag particles. (Microstructure parameters same as for Fig. 14.)

step model of the photoemission described in Sec. II and the extended DEMA of the optical absorption described in Sec. III. We will demonstrate the microstructural effects on the PQY and give evidence of the precision our calculation provides. In our calculation, it is emphasized here that we have taken the multiple elastic scattering events of photoexcited electrons inside the Ag-particle boundaries into consideration. As described in Sec. II, the mean free path of the photoexcited electrons in the Ag is ≈ 1000 Å at the cutoff (threshold) wavelength (1.1 eV or 1.1 μm) of the S-1 photocathode. For a surface layer with particle size of 50 Å, the inclusion of the geometric factor γ [Eq. (10)] due to the elastic scattering of electrons in the particles in the calculation makes the PQY ≈ 20 times larger than that excluding γ. Interestingly enough, the number of multiple elastic scattering of electrons in the particle of 50 Å is ≈ 1000 Å/50 Å, which makes a factor of ≈ 20 as well. Figure 15 exhibits this enhancement factor. The consideration of the geometric factor leads to the results close to the experimental data.[6] Figure 16 reveals the Ag-particle-size effects on the PQY. Since the number of multiple elastic scattering events of an electron in the particle is larger when the particle is smaller, the probability for a photoexcited electron to escape into the vacuum and be collected is therefore also larger. Note that the PQY enhancement at higher photon energies (the peak near 0.41 μm), where the photoelectron mean free path is short and the geometric enhancement factor therefore less important, is due to the higher photoabsorption for smaller particles and the higher transmission coefficient of high energy photoelectrons. On the other hand, the enhancement at lower photon energies is due to multiple elastic scattering.

From Eqs. (17)–(20), we can see the individual contributions of the surface and base layers to the PQY of the S-1 photocathode. Figure 17 shows the PQY of these two layers separately and the total PQY. The corresponding optical absorption is shown in Fig. 14. It is found that the surface layer contributes most to the photoyield. The discrepancy between the features of optical absorption and spectral response curves can thus be accounted for. Before showing the microstructural effects on the spectral response of the S-1 photocathode, it is worth stressing here that the minima around 3.8 eV for all PQY curves represent the plasmon loss as discussed in Sec. III.

The contribution of the second microstructural unit to the PQY is given in Fig. 18(a). We see that as the second unit disappears, the PQY in the near infrared diminishes accordingly. It has been reported by Asao[2,19] that the in-

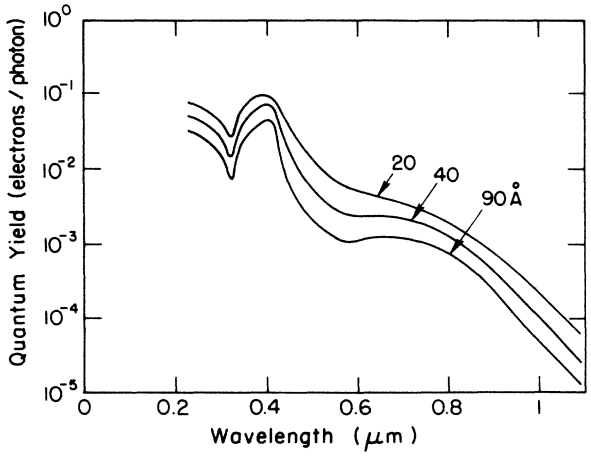

FIG. 16. Dynamic effective-medium calculation of the particle-size effect on the total photoelectric quantum yield of the S-1 photocathode. Note the increasing PQY at decreasing particle-size D. (Other parameters same as Fig. 14.)

creasing amount of silver deposited increases the photoelectric current at $\lambda \approx 0.7$ μm which in our model is attributed to the aggregated of Ag particles. Figure 18(b) reveals the Ag volume fraction effects on the PQY. Obviously, as the Ag volume fraction increases from 40%, 50%, and 60%, the PQY peak in the near infrared shifts toward longer threshold wavelength although the peak intensity near 0.8 μm is lower for larger volume fraction. This trend is somewhat different from the optical absorption property exhibited in Fig. 10 given in previous section where the red shift and the increasing of the second unit peak intensity occur simultaneously.

The threshold wavelength is determined by the Schottky barrier height at the interface between the silver and the cesium oxide. Compared with that at high photon energy, the escape probability of photoexcited electrons near threshold is smaller since they carry less kinetic energy to overcome the energy barrier. This, in a way, puts a limit on shifting the threshold wavelength too much into the infrared unless the Schottky barrier width can be narrowed by impurity doping or field assistance so that tunneling of photoexcited electrons from the metal particle into the vacuum becomes possible at kinetic energy lower than the Schottky barrier height. Otherwise, some other materials providing lower Schottky barrier height will be needed for a photocathode with cutoff wavelength greater than that (1.1 μm) of the S-1 photocathode.

Combining all the microstructural parameters, we can reproduce many other PQY curves representing the S-1 surface of various microstructures. The concurrence of all the microstructural effects can therefore be possibly employed to explain certain PQY curves measured experimentally.[3,5,6] For example, in processing the S-1 photocathode, the additional silver deposition was found to increase the PQY in the near infrared while it shortens the threshold wavelength. As the additional silver is evaporated, both the amount of Ag-particle aggregation and the particle size should increase accordingly.[2,20] At the same time, the effective volume fraction of the silver particle should also increase. From the theoretical results presented above, together with the fact that the energy barrier of the small silver particle may vary for different silvering processes which will therefore affect the threshold wavelength, the increasing Ag volume fraction and amount of aggregated Ag particles may well explain the experimental observation. If the energy barrier heights of the additionally deposited Ag particles are not as low as 1.1 eV (1.1 μm), the cutoff wavelength will certainly shorten although the optical absorption of the surface layer near 0.8 μm in the infrared may still go up due to the formation of the second microstructural unit. The work function of the pure Ag is about 4.9 eV which, upon cesiation, reduces to 1.1 eV. As stated before, the $Cs_{11}O_3$ coating the Ag particles is so thin that it simply lowers the Ag work function contributing little or no part to the

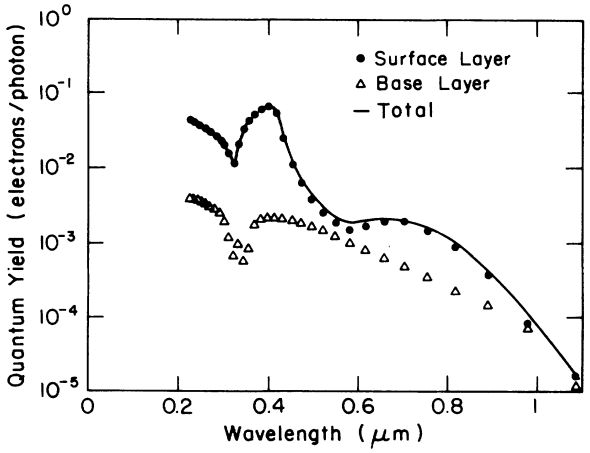

FIG. 17. Comparison of the contribution of total PQY from the surface layer and the base layer. ● Surface layer, △ base layer using DEMA. (All parameters same as Fig. 14.)

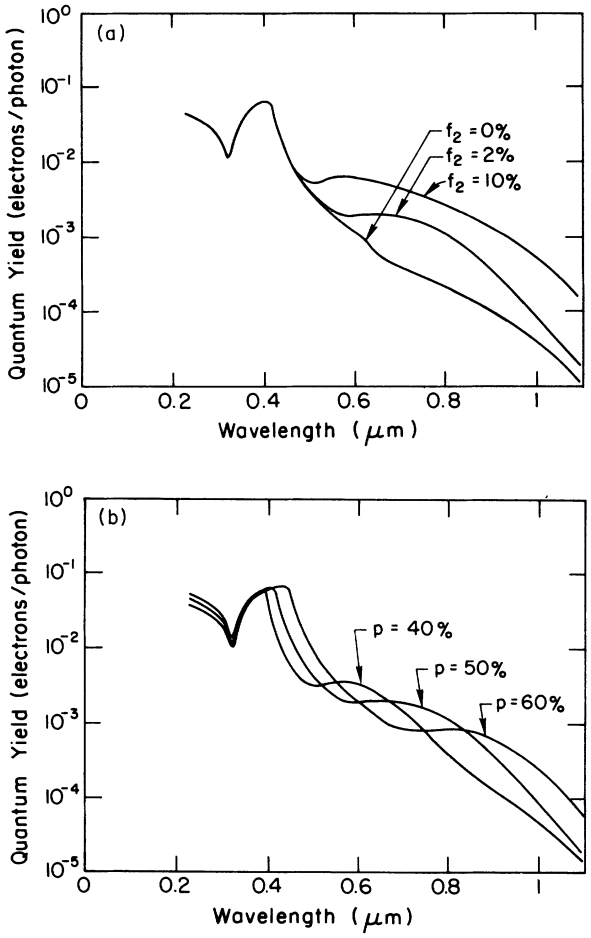

FIG. 18. (a) Ag aggregation (second unit) effect on the PQY of the S-1 surface using DEMA. (Other parameters same as Fig. 14.) (b) Ag-particle volume-fraction effect on the total PQY of the S-1 photocathode using DEMA. (Other parameters same as Fig. 14.)

dielectric constant.

The enhancements of photoabsorption and photoemission all together give rise to the resultant enhanced photoyield. For very large particles the photoabsorption cross section and photoemission yield are low as compared with smaller particles. However, quantum size effects may come into play when the size of a particle is very small. Our classical electrodynamic theory may eventually fail to properly describe its properties. As yet, it is not well understood how particle size affects the work function, the end values for atomic state and bulk state are the ionization energies of atoms which are larger than the ionization energies (i.e., the work functions) of bulk materials. Therefore, the particle size of metal should not be too small so as to lose its metallic nature. For reasonable photoyield, an optimal particle size probably exists.

As a matter of fact, our studies have shown that particle size is not very critical in enhanced photoabsorption especially for particles larger than 20 Å, according to the classical theory. However, for photoemission our theory fails to take into consideration any variation of the work function of Schottky barrier height with particle size. The classic work by Schmidt-Ott and co-workers[33] which showed that a minimum work function exists for particles of 60 Å in diameter suggests that such an effect may occur for Schottky barriers. Recently, there have been studies on the particle-shape effects.[8,34–36] It is found that spheroidal or ellipsoidal particles with smaller minor to major axial ratio show stronger absorptions. Radiation dampings at the tips of these elongated particles are employed to explain these enhancements.[35] In more classic works, this shape effect has also been studied[9,30,37] with similar conclusions.

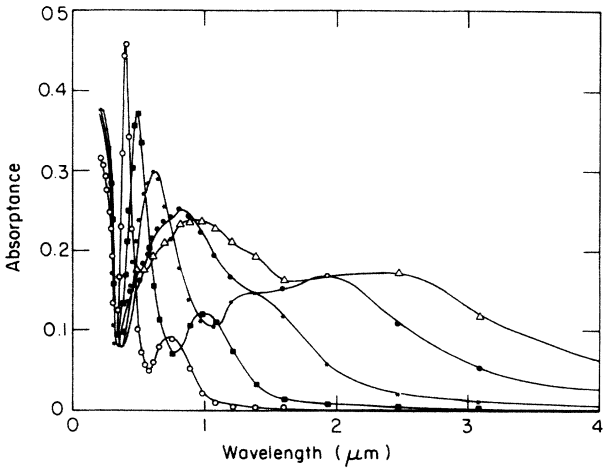

FIG. 19. Dynamic effective-medium calculation of host matrix effects on the photoabsorptions for Ag in various matrices. $d=50$ Å, $H=100$ Å, $p=50\%$, $f_2=2\%$, and $\epsilon_M=1$ (○), 2 (■), 4 (*), 8 (●), and 12 (△).

V. CONCLUSIONS AND MATERIAL DESIGNING RULES

In conclusion, we have proposed a multiple-step model of photoemission that takes the multiple elastic scattering of the photoelectrons in the Ag particles into consideration. Incorporated with the extended dynamic effective medium approximation, this model allows us to calculate the PQY curves for various types of microstructures of the *S*-1 photocathode which represent different stages of processing. Our calculations are done in a more or less precise way since no adjusting factor has been involved. The numerical results seem to agree well with the experimental data. The main features of the PQY and the absorptance of the *S*-1 surface can be interpreted quite successfully.

Based upon the success of this work, we can infer the material-design rules for a heterogeneous composite system with specific optical properties. As demonstrated in Sec. III, it is found that copper and gold particles also show very similar properties such as the anomalous dispersion due to the bounded free electrons as well as the aggregation effects on the optical absorption in the near infrared. We can tailor desired optical properties through selecting adequate microstructural parameters. These parameters include the types of metal particles and their volume fractions, particle sizes, and extent of aggregations of these particles. The semiconductor selected as host matrix also has significant influence on enhancing the photoabsorption of these small metal particles.

The larger dielectric constants of semiconductors imply higher polarizabilities which again indicate that it requires less energy to excite a resonance. Therefore, there is a red shift as the embedding matrix is replaced with a higher dielectric constant semiconductor for the same species of metal particles. Figure 19 indicates this host matrix effect. Besides the significant photoabsorption in the infrared, photoelectrons have to be efficiently collected in some way for photon detection applications. Tunneling of electrons between metal particles is not an efficient way of electron transport as compared with conduction band transport. For fast response we need to provide a medium to collect photoelectrons so that electrons escaping from the metal particles will move in the semiconductor and be collected therein. The energy barriers for electrons to escape and therefore the cutoff photon energy of a photodetecting material also depend on the type of semiconductor chosen. High dielectric constant materials such as Si, GaAs, and $CuInSe_2$2, etc., are good candidates for these purposes. What is important to the selection for the proper host matrix is the ability to fabricate the random heterostructures with various small metal particles without the complication of metal-semiconductor compound formation and/or interdiffusions.

ACKNOWLEDGMENTS

This research was supported by the National Science Foundation under Grant No. ECS 85-20580. Facilities at the Center for Materials Research of Stanford University were used in this investigation.

[1]L. R. Koller, J. Opt. Soc. Am. **19**, 135 (1929).
[2]A. H. Sommer, *Photoemissive Materials* (Wiley, New York, 1968), Chap. 10.
[3]N. Alexander and C. W. Bates, Jr., J. Opt. Soc. Am. A **2**, (11)1848 (1985).
[4]C. W. Bates, Jr., Phys. Rev. Lett. **47**, 204 (1980).
[5]S. J. Yang and C. W. Bates, Jr., App. Phy. Lett. **36**, 675 (1980).
[6]S. J. Yang, Ph.D. dissertation, Stanford University, 1978.
[7]K. U. von Raben, K. C. Lee, R. K. Chang, and R. E. Benner, Jr., J. Appl. Phys. **55**, 3907 (1984).
[8]P. Sheng, Phys. Rev. Lett. **45**, 60 (1980).
[9]C. F. Bohren and D. R. Huffman, *Absorption and Scattering of Light by Small Particles* (Wiley-Interscience, New York, 1983), Chap. 12.
[10]G. Ebbinghaus, W. Braun, and A. Simon, Phys. Rev. Lett. **37** (26), 1770 (1976).
[11]C. W. Bates, Jr., Appl. Phys. Lett. **45**(10), 1058 (1984).
[12]Q. D. Wu, Acta Physica Sinica **28**(4), 553 (1979).
[13]Q. D. Wu, Acta Physica Sinica **29**(5), 608 (1979).
[14]W. Y. Chen and C. W. Bates, Jr., Phys. Rev. Lett. **57**(21), 2737 (1986).
[15]N. V. Smith, CRC Critical Review in Solid State Science, March, 1971.
[16]D. Stroud and F. P. Pan, Phys. Rev. B **17**, 1602 (1978).
[17]N. V. Alexander and C. W. Bates, Jr., Solid State Commun. **51**(5), 331 (1984).
[18]H. Kanter, Phys. Rev. B **1**(2), 522 (1970).
[19]S. Asao, Proc. Phys. Math. Soc. Jpn. **22**, 448 (1940).
[20]O. S. Heavens, *Optical Properties of Thin Solid Films* (Dover, New York, 1965).
[21]P. B. Johnson and R. W. Christy, Phys. Rev. B **6**(12) 4370 (1972).
[22]F. Wooten, *Optical Properties of Solids* (Academic, New York, 1972).
[23]T. H. Hodgson, Proc. Phy. Soc. **68**, 593 (1955).
[24]H. C. Van de Hulst, *Light Scattering by Small Particles* (Academic, New York, 1981).
[25]M. Kerker, *The Scattering of Light and Other E. M. Radiations* (Academic, New York, 1969).
[26]N. V. Alexander, Ph.D dissertation, Stanford University, 1986 (unpublished).
[27]P. Chylek and V. Srivastava, Phy. Rev. B **27**, 5089 (1983).
[28]S. Yamaguchi *et al.*, Surf. Sci. **138**, 449 (1984).
[29]F. S. Crawford, Jr., *Waves* (McGraw-Hill, New York, 1968).
[30]A. E. Hughes and S. C. Jain, Adv. Phys. **28**(6), 717 (1979).
[31]W. Jones and N. H. March, *Theoretical Solid State Physics* (Wiley-Interscience, London, 1973), Vols. I and II.
[32]S. Ichimaru, *Plasma Physics* (Benjamin-Cumming, Menlo Park, California, 1986).
[33]A. Schmidt, P. S. Schurtenberger, and H. C. Siegman, Phys. Rev. Lett. **45**(15), 1284 (1980).
[34]L. C. Chu and S. Y. Wang, J. Opt. Soc. Am. **2**(6), 950 (1985).
[35]L. C. Chu and S. Y. Wang, Phys. Rev. B **31**(2), 695 (1985).
[36]A. Wokun, J. P. Gordan, and P. F. Liao, Phys. Rev. Lett. **48**(14), 957 (1982).
[37]D. C. Skillman and C. R. Berry, J. Chem. Phys. **48**, 3297 (1968).